A boundary element formulation for acoustic shape sensitivity analysis

J. H. Kane and S. Mao
Mechanical and Aeronautical Engineering, Clarkson University, Potsdam, New York 13699

G. C. Everstine
David Taylor Research Center, Bethesda, Maryland 20814-5000

(Received 18 October 1990; accepted for publication 15 March 1991)

The Helmholtz integral equation forms a conventional basis for acoustic boundary element analysis (BEA). Implicit differentiation of the discretized Helmholtz integral equation is shown to yield an effective approach for the computation of rates of change (sensitivities) of acoustic response quantities with respect to changes in the shape of an acoustic model. A theoretical formulation is presented that allows for the reuse of the factorization of the overall BEA system left-hand side matrix formed in a previous analysis, thus obviating the need to factor perturbed matrices in the sensitivity analysis process. The singularity strengths of the new kernel functions utilized to compute sensitivities of matrix coefficients required by this approach are shown to be the same as those present in ordinary BEA. An indirect approach for the computation of the diagonal contributions to sensitivity matrices associated with these new kernels is also discussed. The sensitivity analysis formulation includes surface pressures and normal gradients (velocities), surface tangential pressure gradients, and pressure and pressure gradients at arbitrary domain sample points. It is concluded that the overall efficiency of implementations of these formulations is significant. Numerical results for a series of example problems are presented to quantify the accuracy and efficiency of this approach.

PACS numbers: 43.20.Rz, 43.20.Ks, 43.30.Jx, 43.40.Rj

INTRODUCTION

The process of computing rates of change of response quantities associated with an object with respect to changes in the parameters (design variables) that control its shape has been termed design sensitivity analysis (DSA). These derivatives (sensitivities) are used in shape optimization by numerical optimization procedures to determine effective search directions and move lengths in the space of these design variables. Economical and accurate DSA computation is a pacing item in the attempt to make large scale shape optimization tractable. Implicit differentiation[1–12] of discretized boundary integral equations has been shown to be an effective strategy for the formulation of DSA relations in two-dimensional linear and nonlinear heat transfer and stress analysis. The major advantage of this approach is that it obviates the requirement to factor perturbed left-hand side matrices, but instead, allows for the multiple reuse of the LU factorization of the current BEA system matrix formed during the last analysis.

The use of boundary elements (in today's terminology) to solve acoustics problems dates back almost 30 years to the work of Chen and Schweikert[13] and Chertock.[14] Except for the early years, most of the work in this area has been based on the Helmholtz boundary integral equation (a direct boundary element method) rather than on a simple source approach (an indirect boundary element method). The primary reason for this choice is that the singularities which arise at the characteristic frequencies of the integral equation are associated with nonexistence of the solution in the indirect formulation and nonuniqueness in the direct formulation. Both Schenck[15] and Burton and Miller[16] developed methods to avoid these singularities, and variants of their procedures continue to be used today. Other developments over the intervening years have included the extension to higher-order (e.g., quadratic) fluid shape functions,[17–19] the introduction of special techniques suitable for axisymmetric geometries,[20,21] and the coupling of boundary element fluid models with finite element and boundary element models of elastic structures[19,20,22–24] for the solution of fluid-structure interaction problems. We are not aware of any previous work involving shape sensitivity analysis for boundary element acoustic analysis. We view the current work as the first step in the ability to perform shape optimization in acoustics and structural acoustics.

At the matrix level, the two-dimensional acoustic shape DSA formulation is identical to its counterpart in thermal and structural analysis. This paper will therefore focus mainly in the distinctive new aspects that are introduced due to the acoustic character of the BEA approach employed. A theoretical formulation for the entries in the matrix sensitivities required in the implicit differentiation approach is given, that includes sensitivities of acoustic fundamental pressure and pressure normal gradient (velocity) solutions, unit normal vectors, and boundary element Jacobians. This formulation employes quadratic, singular, isoparametric boundary elements, and is sufficient for the computation of the sensitivities of unknown boundary pressures and pressure normal gradients on the surface of the BEA model. These matrix

sensitivities are shown to exhibit significant sparsity for objects with partial geometric sensitivity. The exploitation of this sparsity is shown to yield considerable savings in computation. A formulation for the recovery of sensitivities of tangential pressure gradient components on the surface of the model is also presented, that does not require any additional numerical integration. Formulas for the recovery of pressure and pressure gradient components at interior (domain) sample points is also presented. A series of example problems are presented for which analytical sensitivity formulas exist. Computed sensitivities are compared to these analytic sensitivities and CPU timings are reported.

I. ACOUSTIC BOUNDARY ELEMENT ANALYSIS FORMULATION

A concise integral formulation[25-27] is presented to serve as the basis for the sensitivity analysis that follows. In steady harmonic acoustic BEA, the fundamental solution, symbolized by p^*, refers to the response of an infinite acoustic medium, with acoustic wave number k, to a unit point source of excitation. Mathematically, this point source at location $\mathbf{d}$ is represented by a Dirac delta function $\delta(\mathbf{x}-\mathbf{d})$ at sample point $\mathbf{x}$. A governing boundary integral equation can be derived by substituting p^* for g in Green's second identity shown below, and choosing f to be the pressure response of the actual problem under consideration. In this discussion, Ω is the domain of the actual problem, Γ is the boundary of this domain and $\mathbf{n}$ is the unit outward normal vector on the surface, and c is a constant that depends on whether the source point $\mathbf{d}$ is inside, outside, or on the boundary of the problem. The symbol q^* denotes the normal component of the pressure gradient vector corresponding to the fundamental pressure solution. Use of the selection property of the delta function has also been made here:

$$\int_\Omega \nabla^2 fg\, d\Omega - \int_\Omega \nabla^2 gf\, d\Omega = \int_\Gamma g\, \nabla f\cdot\mathbf{n}\, d\Gamma - \int_\Gamma f\, \nabla g\cdot\mathbf{n}\, d\Gamma, \tag{1}$$

$$\nabla^2 p^* + kp^* = \delta(\mathbf{x}-\mathbf{d}), \tag{2}$$

$$cp(\mathbf{d}) + \int_\Gamma p^* q\, d\Gamma = \int_\Gamma q^* p\, d\Gamma. \tag{3}$$

In the above formulation, an incident pressure p^i could also be included to treat scattering problems. Equation (3), the Helmholtz integral equation, can be discretized by breaking the surface into a number of boundary elements, and approximating the geometry, boundary conditions, and unknown response using simple interpolating functions and the values of these quantities at a finite number nodes:

$$cp(\mathbf{d}) + \sum_{E=1}^{NEL} \left(\int_{-1}^{+1} p^*\{H\}J\, da\right)^{(E)} \{q\}^{(E)} = \sum_{E=1}^{NEL} \left(\int_{-1}^{+1} q^*\{H\}J\, da\right)^{(E)} \{p\}^{(E)}. \tag{4}$$

In this expression, $\{H\}$ is a row vector of element interpolation functions associated with each node on element E, a is an element intrinsic coordinate that runs from -1 to $+1$ in each element, and J is the Jacobian of the transformation from the actual differential length $d\Gamma$ to da in the element's intrinsic coordinate system. Here, $\{p\}^{(E)}$ and $\{q\}^{(E)}$ are column vectors of the node point pressures and normal pressure gradient components, respectively, for element E and have been taken outside the integrals shown to produce an algebraic expression. This boundary integral equation can be written for any location of the source point of the fundamental solution. A singular boundary element formulation is obtained by locating this point at each of the nodes in the model, producing a square system of algebraic equations.

$$[F]\{p\} = [G]\{q\}. \tag{5}$$

In this expression, $\{p\}$ is a column vector of nodal point pressures and $\{q\}$ is a vector of nodal point normal pressure gradient components. The matrix $[F]$ is square, and $[G]$ is either square or rectangular.

In a well-posed boundary value problem, half of the pressures and normal pressure gradient components will be specified (and therefore known) and the other half will be unknown. By transferring all known values to the right-hand side (rhs) vector $\{q\}$, placing all unknown pressures and normal pressure gradient components in the lhs vector $\{p\}$, exchanging corresponding columns of the respective rectangular matrices, and performing the indicated matrix-vector multiplication on the rhs, a solvable system of equations can be produced. This equation is usually solved by triangular factorization of the matrix $[A]$ using a Gauss elimination procedure with partial pivoting, followed by forward reduction of $\{b\}$ and backward substitution to determine the unknown response vector $\{x\}$:

$$[A]\{x\} = \{b\}. \tag{6}$$

Note that the notation has been generalized to mean that $\{p\}$ is the vector of unknown boundary response quantities, while $\{q\}$ denotes the vector of specified boundary conditions. At each node, if q has been specified, then $\{p\}$ contains p, while if p had been specified then $\{p\}$ contains q for this entry.

II. SENSITIVITY FORMULATION FOR PRESSURES AND NORMAL PRESSURE GRADIENT COMPONENTS

As shown in Refs. 1 and 2, implicit differentiation of the algebraic system equations that result when the discretized boundary integral equations are written for a set of load point locations corresponding to boundary element nodes yields

$$\frac{\partial}{\partial X_L}([F]\{p\} = [G]\{q\}) \tag{7}$$

or

$$[F]\{p\}_{,L} = ([G]_{,L}\{q\} - [F]_{,L}\{p\}). \tag{8}$$

In the above expression, X_L represents the L th design variable. Equation (8) reveals a fundamental characteristic of the implicit differentiation approach to DSA. *If the right-hand side vector shown can be formed, then the unknown nodal response sensitivity vector $\{p\}_{,L}$ can be determined by simply solving Eq. (8), by forward reduction and back substitution, using the factorization of the left-hand side matrix $[F]$ computed in the previous analysis step.*

The entries in the matrix sensitivities shown in Eq. (8)

are assembled from contributions associated with pairs of elements and load points as

$$[F]_{,L}^{(E,P)} = \int_{-1}^{+1} (q_{,L}^* \{H\}J + q^* \{H\}J_{,L}) da \tag{9}$$

and

$$[G]_{,L}^{(E,P)} = \int_{-1}^{+1} (p_{,L}^* \{H\}J + p^* \{H\}J_{,L}) da; \tag{10}$$

$p_{,L}^*$ and $q_{,L}^*$ are sensitivities of the fundamental pressure and normal pressure gradient component solutions, respectively, for the acoustic problem for element E due to a unit point excitation load point P. $J_{,L}$ is the sensitivity of the Jacobian for the transformation from the real element coordinates x_i to the intrinsic (isoparametric) coordinates a, for example, as shown for the three-noded continuous element in Fig. 1. $\{H\}$ is a 1×3 matrix of interpolation (shape) functions $h^{(n)}$ for the three-node isoparametric element. Sensitivity expressions for these quantities are

$$p_{,L}^* = (-ik/4)H_1^1(kR)R_{,L} \tag{11}$$

and

$$q_{,L}^* = (-ik/4R)\{b_{,L}H_1^1(kR) + bR_{,L}[kH_0^1(kR) - 2H_1^1(kR)R^{-1}]\}, \tag{12}$$

where

$$y_i = x_i - d_i; \quad y_{i,L} = x_{i,L} - d_{i,L}, \tag{13}$$

$$R = \{y_i y_i\}^{1/2}; \quad R_{,L} = R^{-1} y_i y_{i,L}, \tag{14}$$

$$n_1 = J^{-1} x_{2,a}; \quad n_2 = -J^{-1} x_{1,a}; \tag{15}$$

$$n_{1,L} = -J^{-2} J_{,L} x_{2,a} + J^{-1} x_{2,aL};$$

$$n_{2,L} = +J^{-2} J_{,L} x_{1,a} - J^{-1} x_{1,aL}, \tag{16}$$

$$x_i = \sum_{N=1}^{3} h^{(N)} x_i^{(N)}; \quad x_{i,a} = \sum_{N=1}^{3} h_{,a}^{(N)} x_i^{(N)}, \tag{17}$$

$$x_{i,L} = \sum_{N=1}^{3} h^{(N)} x_{i,L}^{(N)}; \quad x_{i,aL} = \sum_{N=1}^{3} h_{,a}^{(N)} x_{i,L}^{(N)}, \tag{18}$$

$$J = \{x_{i,a} x_{i,a}\}^{1/2}; \quad J_{,L} = J^{-1} x_{i,a} x_{i,aL}, \tag{19}$$

$$b = n_i y_i; \quad b_{,L} = n_{i,L} y_i + n_i y_{i,L}, \tag{20}$$

and

$$H_i^j(kR) = \text{Hankel function of the } j\text{th kind of order } i. \tag{21}$$

In these expressions, R is the distance from the load point $\mathbf{d}$ to the sample point $\mathbf{x}$, and $\mathbf{n}$ is the unit outward normal to the surface at $\mathbf{x}$. In the derivation of the above formulas, use has also been made of the relations

$$p^* = (i/4)H_0^1(kR); \quad q^* = -(ibk/4R)H_1^1(kR), \tag{22}$$

$$\frac{d}{dR} H_0^1(kR) = -kH_1^1(kR), \tag{23}$$

$$\frac{d}{dR}[RH_1^1(kR)] = kRH_0^1(kR). \tag{24}$$

One might suspect that the differentiation of the fundamental solutions present in the BEA formulation would lead the development of integral equations for DSA that were more singular than the original ones. Remarkably, this is not the case. Examination of Eqs. (9)–(21) reveals that *the functions involved in the DSA formulation have exactly the same singularity characteristics as those present in the original analysis step.* That is to say, $p_{,L}^*$ and $q_{,L}^*$ contain functions that behave like $\ln(R)$ and R, respectively, as this distance approaches zero. The behavior of q^* (and thus $q_{,L}^*$) is due to the orthogonality of $\mathbf{n}$ and $\mathbf{y}$ (at a rate of order R^2) when $\mathbf{d}$ approaches $\mathbf{x}$ and the R^{-1} behavior of $H_1^1(kR)$ as shown in Hildebrand.[28] The supposition about $p_{,L}^*$ is verified by observing in Eq. (14) that $R_{,L}$ approaches 0 like R when $\mathbf{d}$ approaches $\mathbf{x}$. This property is due to the fact that $y_{i,L}$ approaches zero as $\mathbf{d}$ approaches $\mathbf{x}$. These characteristics allow numerical integration techniques (sets of sample points and associated weighting coefficients), developed for standard BEA, to be employed in this DSA step without modification. This statement is true for both the so-called outside integration (R never becomes zero for a particular E, P combination) and inside integration (R becomes zero for a particular E, P combination) process.

The numerical integration process indicated in Eqs. (9) and (10) deserves some further comment. These two term expressions, at first, appear to be considerably more computationally burdensome than their counterparts in BEA. However, further examination of these expressions reveals that this is not the case. Note that only the steps associated with the computation of sensitivities of the fundamental solutions and the sensitivity of the Jacobian and normals are extra. Also, even in these formulas, about half of the quantities present are not sensitivities. Note further that the arithmetic operations associated with the formation of the 1×3 matrix products remains identical to the operations utilized in standard BEA. For problems in which a considerable portion of the surface is geometrically insensitive to the design variable, significant savings in computational effort can be accomplished in this DSA integration step, due to the fact that the matrix sensitivities will be sparse. In subsequent sections, numerical examples will be presented to demonstrate these assertions regarding computational efficiency.

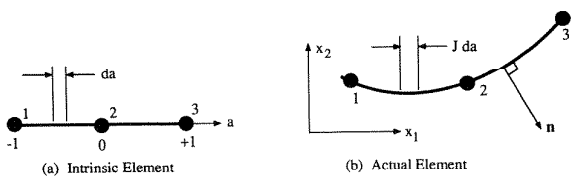

FIG. 1. Three node isoparametric continuous boundary element.

III. STRONGLY SINGULAR INTEGRATIONS FOR CURVED SIDED ELEMENTS

The direct method of acoustic (BEA) involves the generation of a square system of algebraic equations. Each row of these algebraic equations is associated with a different location of the source point of a discretized boundary integral equation. In singular BEA formulations, these source points are located precisely at the node points of the BEA

model, thus requiring that the source point and sample point present in the boundary integral equations to coincide for the case when the source point as on the boundary element being integrated. This case is generally referred to as inside integration. These fundamental solutions (in 2D) are Hankel functions that behave like $\ln(R)$ and R^{-1}, where "R" is the distance between the source and sample points. The logarithmic behavior is known to be only weakly singular, while the R^{-1} function is known to be singular (sometimes called strongly singular). The orthogonality property, discussed above, between **n** and **y** will smooth out the singularity present in q^*. Numerical integration of the logarithmically singular functions is possible by suitable clustering of the integration sample points and adjusting of the corresponding weighting coefficients.[25–27] The numerical integration of the functions that contain contributions that behave like R^{-1} can also be handled by an indirect approach. This approach to the performance of this type of integration is to use some known solution to the physical problem to indirectly obtain the values of the coefficients associated with this integration.

In this section, it is shown that the value of terms associated with the inside integration process can also be obtained from another *indirect* process for both the analysis and for DSA. This indirect process relies on certain physical properties of the response of the continuum acoustics problem. In steady harmonic acoustics, use can be made of the fact that certain known solutions to problems exist. For example, plane-wave and cylindrical-wave solutions to the 2-*D* Helmholtz equation are well known. To understand how the indirect integration process works, it is also necessary to realize that the integrations done in BEA involve purely geometric information. That is to say, the same integrations would be performed in the analysis of two geometrically identical BEA models with different boundary conditions. These considerations allow for the deduction of a relationship among the $[F]^{(E,P)}$ and $[G]^{(E,P)}$ contributions to the overall BEA matrices. To derive this relationship, it is necessary to imagine a *hypothetical* problem that has geometrically identical boundaries to the actual problem under consideration. In this hypothetical problem, let the boundary condition at each node be a specified pressure and normal gradient equal to, for instance, the plane-wave solution. The overall BEA algebraic equations for this hypothetical problem become

$$[F]\{\tilde{p}\} = [G]\{\tilde{q}\}. \tag{25}$$

The tilde symbol is used to denote known quantities associated with the plane-wave solution. This matrix equation actually contains "N" equations, one for each row in the matrix. Writing this relation for the ith row in the matrix, a property of each row of the matrix is established:

$$\sum_{k=1}^{N} f_{ik}\tilde{p}_k = \sum_{k=1}^{N} g_{ik}\tilde{q}_k. \tag{26}$$

Each row in the BEA matrices correspond to a different location of the source point. In the singular BEA formulation, this means that each row in the BEA matrices corresponds to a source point location at a different node. The columns in BEA matrices are also associated with different nodes. Therefore, *when the row and column number coincide, this represents the case of the source point being at the corresponding node in the element during the integration process* (i.e., inside integration). Thus the diagonal entry of the $[F]$ matrix is the entry that is formed in the inside integration process. Extracting this term from the sum shown in Eq. (26) yields a so-called row sum property:

$$f_{mm} = \tilde{p}_m^{-1}\left(\sum_{k=1}^{N} g_{mk}\tilde{q}_k - \sum_{\substack{k=1\\k\neq m}}^{N} f_{mk}\tilde{p}_k\right). \tag{27}$$

In DSA, an *indirect approach can again be employed to compute the Cauchy principal values associated with the diagonal terms of the* $[F]_{,L}$ *matrix*. This is accomplished by taking the derivative of Eq. (27) with respect to X_L:

$$\begin{aligned} f_{mm,L} = &-\tilde{p}_m^{-2}\tilde{p}_{m,L}\left(\sum_{k=1}^{N} g_{mk}\tilde{q}_k - \sum_{\substack{k=1\\k\neq m}}^{N} f_{mk}\tilde{p}_k\right)\\ &+\tilde{p}_m^{-1}\left(\sum_{k=1}^{N} g_{mk,L}\tilde{q}_k - \sum_{\substack{k=1\\k\neq m}}^{N} f_{mk,L}\tilde{p}_k\right)\\ &+\tilde{p}_m^{-1}\left(\sum_{k=1}^{N} g_{mk}\tilde{q}_{k,L} - \sum_{\substack{k=1\\k\neq m}}^{N} f_{mk}\tilde{p}_{k,L}\right). \end{aligned} \tag{28}$$

Note that this expression describes a generalized row sum property involving the coefficients of the analysis matrices as well as their sensitivities. The sensitivities of the general horizontal plane-wave solution are

$$\tilde{p}_{,L} = ik(\cos kx_1 + i\sin kx_1)x_{1,L}, \tag{29}$$

$$\tilde{q}_{,L} = k\,[-k(\cos kx_1 + i\sin kx_1)x_{1,L}n_1 + (i\cos kx_1 - \sin kx_1)n_{1,L}]. \tag{30}$$

Cylindrical-wave solutions to the hypothetical acoustic problem have also been used to determine the Cauchy principal values in both analysis and DSA. These solutions, however, involve Hankel functions and are marginally more computationally burdensome.

It is also noted here that the diagonal entry of the $[F]$ matrix may not, in general, be due only to the influence of a point on itself (sometimes referred to as the "self" terms) since, for a domain with a plane of symmetry, the diagonal entries include the effects of image points. This case can also be accommodated by the formulation described above.

IV. SENSITIVITY FORMULATION FOR TANGENTIAL COMPONENTS OF SURFACE PRESSURE GRADIENTS

As depicted in Eqs. (7) and (8), the quantities involved in this DSA formulation at the algebraic equation solving level are sensitivities of node point pressure and boundary normal pressure gradient components. In acoustic problems, the tangential component of the pressure gradient may also be of interest, for example, to verify computed solutions by comparison with classical results. In thermal problems this quantity is analogous to the tangential heat flux, and in structural problems the counterpart to this quantity is the membrane component of the stress tensor. This quantity is also important in sensitivity analysis research because it is

generally the least accurate, thus providing a harsh test for any particular formulation and implementation. The formulas for recovery of tangential pressure gradient component information on the surface of a BEA model can be differentiated with respect to X_L to generate a sensitivity formulation for these quantities. Care must be taken to recognize all of the possible geometric and acoustic quantities that can be sensitive to the design variable, and to include these derivatives in this differentiation process.

Figure 2 can be used to visualize the coordinate systems involved in the tangential pressure gradient component recovery and subsequent sensitivity recovery process. In the global x_i coordinate system we have q_i as the ith component of the pressure gradient vector. In the local (tangential and normal) z_i coordinate system, located at the node where the tangential pressure gradient is to be recovered, s_i is used to symbolize these corresponding components. This local coordinate system is configured so that the z_2 direction is tangent to the boundary element and pointing in the direction of increasing a, and z_1 is normal to the element. In this local coordinate system, the following relationships exist:

$$s_1 = \frac{\partial p}{\partial n} = q; \quad s_{1,L} = q_{,L} \tag{31}$$

$$s_2 = \frac{\partial p}{\partial z_2} = \frac{\partial p}{\partial a}\frac{\partial a}{\partial z_2} = p_{,a}J^{-1};$$

$$s_{2,L} = p_{,aL}J^{-1} - J^{-2}J_{,L}p_{,a}, \tag{32}$$

where

$$p_{,a} = \sum_{N=1}^{3} h_{,a}^{(N)}p^{(N)}; \quad p_{,aL} = \sum_{N=1}^{3} h_{,a}^{(N)}p_{,L}^{(N)} \tag{33}$$

and

$$q_i = l_{ji}s_j; \quad q_{i,L} = l_{ji,L}s_j + l_{ji}s_{j,L}. \tag{34}$$

In the above expressions, $p^{(N)}$ are the node point pressures for the element under consideration, and l_{ij} are direction cosines associated with the coordinate transformation. The l_{ij} components are all derivable from n_i. All of the vector components shown above, with the exception of Eq. (34) are resolved in the local coordinate system. Equation (34) is the transformation of the normal and tangential components of these physical entities back to the global coordinate system. The physical interpretation of this expression for the sensitivities of the pressure gradient components in the global coordinate system is straightforward. The first term on the right-hand side of Eq. (34) determine the sensitivity of q_i due to a change in orientation of the local coordinate system, with the local gradient s_j remaining constant. The last term in Eq. (34) determines the sensitivity of q_i due to a change in the local pressure gradient s_j, with the orientation of the local coordinate system remaining constant. The development of a relationship for the boundary velocity components is also straightforward:

$$v_i = (-1/i\omega\rho)q_i; \quad v_{i,L} = (-1/i\omega\rho)q_{i,L}. \tag{35}$$

In this expression, ω is the excitation circular frequency and ρ is the fluid mass density.

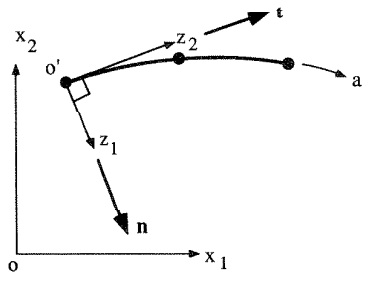

FIG. 2. Coordinate system involved in tangential pressure gradient recovery.

V. DOMAIN POINT SENSITIVITY ANALYSIS

Integral relations are well known for the recovery of pressure and pressure gradient components at sample points in the domain (interior) of a BEA model. These integral equations can be differentiated to yield new integral equations for the recovery of the sensitivities of pressure and pressure gradient components to changes in the design variable. The integral equations that result involve the boundary response (nodal pressure and pressure gradient components) and the sensitivity of these response quantities. Thus the recovery of internal point sensitivities can be accomplished via a boundary integration process completely analogous to that performed in the original BEA process. This formulation is shown below:

$$\begin{aligned} p_{,L}(\mathbf{d}) = &\sum_{E=1}^{NE}\left(\int_{-1}^{+1}(p_{,L}^*\{H\}J + p^*\{H\}J_{,L})da\right)\{q\}^{(E)} \\ &- \sum_{E=1}^{NE}\left(\int_{-1}^{+1}(q_{,L}^*\{H\}J + q^*\{H\}J_{,L})da\right)\{p\}^{(E)} \\ &+ \sum_{E=1}^{NE}(p^*\{H\}J\,da)\{q_{,L}\}^{(E)} \\ &- \sum_{E=1}^{NE}(q^*\{H\}J\,da)\{p_{,L}\}^{(E)}, \end{aligned} \tag{36}$$

$$\begin{aligned} -q_{i,L}(\mathbf{d}) = &\sum_{E=1}^{NE}\left(\int_{-1}^{+1}(p_{,iL}^*\{H\}J + p_{,i}^*\{H\}J_{,L})da\right)\{q\}^{(E)} \\ &- \sum_{E=1}^{NE}\left(\int_{-1}^{+1}(q_{,iL}^*\{H\}J + q_{,i}^*\{H\}J_{,L})da\right)\{p\}^{(E)} \\ &+ \sum_{E=1}^{NE}\left(\int_{-1}^{+1}p_{,i}^*\{H\}J\,da\right)\{q_{,L}\}^{(E)} \\ &- \sum_{E=1}^{NE}\left(\int_{-1}^{+1}q_{,i}^*\{H\}J\,da\right)\{p_{,L}\}^{(E)}. \end{aligned} \tag{37}$$

The sensitivities of many of the quantities in Eqs. (36) and (37) have been defined, except for the ones shown below:

$$p_{,i}^* = q_i^* = (ki/4R)y_iH_1^1(kR), \tag{38}$$

$$\begin{aligned} p_{,iL}^* = q_{i,L}^* = (ki/4R)\{&y_{i,L}H_1^1(kR) + y_i[kH_0^1(kR) \\ &- 2R^{-1}H_1^1(kR)]R_{,L}\}, \end{aligned} \tag{39}$$

$$\begin{aligned} q_{,i}^* = (ki/4R)\{&n_iH_1^1(kR) \\ &+ by_iR^{-1}[kH_0^1(kR) - 2R^{-1}H_1^1(kR)]\}, \end{aligned} \tag{40}$$

$$q^*_{,iL} = (ki/4)(n_{i,L}R^{-1}H^1_1(kR) + n_i[R^{-1}H^1_1(kR)]_{,R}R_{,L} + \{by_iR^{-2}[kH^1_0(kR) - 2R^{-1}H^1_1(kR)]\}_{,L}), \quad (41)$$

where

$$c = R^{-1}[kH^1_0(kR) - 2R^{-1}H^1_1(kR)], \quad (42)$$

$$f_{,L} = R^{-1}\{b_{,L}cy_i + b[c_{,L}y_i + c(y_{i,L} - y_iR^{-1}R_{,L})]\}, \quad (43)$$

$$c_{,L} = -R^{-1}R_{,L}\{k[R^{-1}H^1_0(kR) + kH^1_1(kR)] - 2[R^{-2}H^1_1(kR) - c]\}. \quad (44)$$

Again, one might suspect that the differentiation of the fundamental solutions undertaken in the interior point sensitivity formulation would lead to the development of integral equations that are more singular than the corresponding original ones. As mentioned earlier, however, this is not the case. Further examination of these equations reveals that *the functions involved in this interior point DSA formulation have exactly the same singularity characteristics as those present in the original analysis step.* Thus numerical integration techniques developed for recovery of interior point response information in standard BEA can be employed in this DSA step without modification. The numerical integration process indicated in Eqs. (36) and (37), appears to be considerably more computationally burdensome than the corresponding operating in BEA. This is not *entirely* the case. One could argue that about twice the computational work should be required in this process, compared to interior point response recovery in the original BEA, due to the fact that both the surface response and its sensitivity is involved in the computation. Closer examination of the last two terms in either Eqs. (36) or (37), however, reveals an interesting characteristic. The integrations indicated in *these terms are exactly the same integrations that would be performed in the original BEA internal point response recovery process. Thus, if these coefficients are saved and reused in the DSA step, their recomputation can be avoided.* For problems in which a significant portion of the surface is geometrically insensitive to the design variable, significant savings in computational effort can again be accomplished in this DSA integration step for interior point response, due to the fact that many of the terms in Eqs. (36) and (37) will be zero for a significant number of the elements comprising the overall BEA model.

VI. EXAMPLE PROBLEMS

In order to demonstrate the accuracy and efficiency of the formulation presented above, a series of example problems is presented. All example problems were run on the same dedicated computer system with a UNIX operating system using the same FORTRAN 77 compiler and compiler options. Two physical problems were chosen for the demonstrations, each with well-known analytical solutions. First, the problem of a plane rectangular acoustic medium was studied. This model was subjected to an arbitrary pressure amplitude, independent of the x_2 dimension, along its left side, and a different but arbitrary pressure along its right side. The top and bottom surfaces were constrained to have a zero normal pressure gradient. This response in this problem is a plane wave. Second, the response of an annular circular cylindrical region subjected to arbitrary axisymmetric pressure distributions on the inner and outer radii was examined. The straight sides of this model were constrained to have a zero normal pressure gradient to simulate planes of symmetry present in this partial model of a full annular acoustic region. The response to this problem is a cylindrical wave. Figures 3 and 4 shows the geometry and boundary conditions imposed on the BEA models discussed. A series of analyses and design sensitivity analyses were performed based upon these physical problems. In the rectangular problem, the length L was chosen as the design variable. In the cylindrical problem, the inner radius a was chosen as the design variable. The plane analytical solutions for pressure and pressure gradients were then differentiated to yield exact analytical expressions for these sensitivities to changes in the design variables.

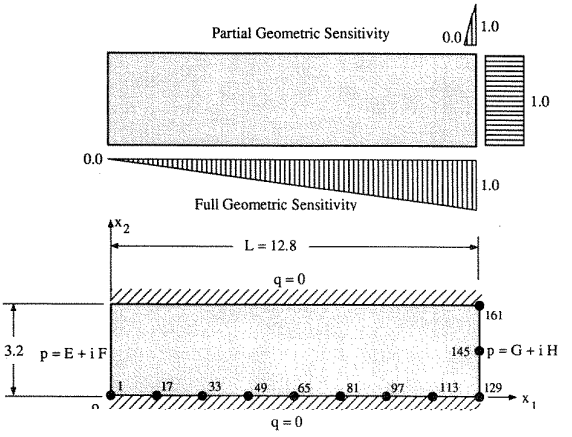

FIG. 3. Plane rectangular region example problem.

It is important to mention that the derivatives computed in this implicit differentiation DSA approach are true material derivatives, including the change in the response field and the possible change in the sample point location induced

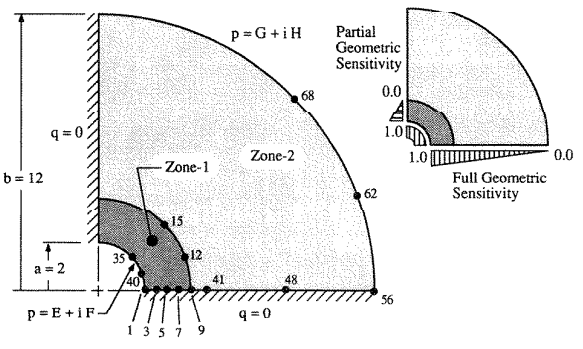

FIG. 4. Plane annular region example problem.

by the change in the design variable. Thus any differentiation of an exact analytical expression must also be a material differentiation, performed by first parametrizing the sample point location in the exact expressions in terms of the design variable and then taking due regard for this derivative in the differentiation process. Figures 3 and 4, for example, show two different schemes that can be employed to control sets of sample (node) point locations, both based upon the value of the design variable. The *full* geometric sensitivity scheme has all nodes along the sides of the respective BEA models geometrically sensitive to the design variable. In the cylindrical model, this radial geometric sensitivity varies in a linear fashion from zero at $R = a$ to unity at $R = b$. In the rectangular problem, the model's x_1 nodal point locations varied in a linear fashion from $x_1 = 0$ to $x_1 = L$. The second schemes, depicted in these figures, has only the nodes in the outward-most row of elements geometrically sensitive to the design variable. Note that a change in these design variables will cause an identical change in the actual response fields simulated by either the full or partially sensitive BEA models. However, because the nodes present in these two BEA models move to different locations in this response field, the node point sensitivities will be different. Nodes in the inner and outer radius of the cylinder models, and nodes on the left and right faces of the rectangular model, will have identical response sensitivities because these nodes have identical geometric sensitivities in both the full and partial geometric sensitivity scheme.

A. Case 1: Rectangular model with full geometric sensitivity

Figure 3 shows the single zone BEA model used in the rectangular region demonstration problems. This rather fine model contained 320 nodes and 160 three-node isoparametric continuous elements. This fine model was studied to provide realistic timing statistics for the steps involved in the analysis and DSA. The arbitrary pressure boundary conditions on the left and right ends of this rectangular region, shown in Fig. 3, were $E = 100$, $F = 200$, $G = 20$, and $H = 30$. Note that these specified values remain the same when the design variable L is changed. This problem was chosen because an exact, closed-form solution to the Helmholtz differential equation exists for these boundary conditions. The physical constants used in this example are $k = \omega = \rho = 1$. The analytical pressure sensitivity solution for this problem is

$$p_{,l} = [-Ekx_{1,L} + B_{,L}]\sin(kx_1) + kBx_{1,L}\cos(kx_1) + i\{[-Fkx_{1,L} + D_{,L}]\sin(kx_1) + kDx_{1,L}\cos(kx_1)\}, \tag{45}$$

where

$$B = [G - E\cos(kL)]/\sin(kL);$$
$$D = [H - F\cos(kL)]/\sin(kL), \tag{46}$$
$$B_{,L} = kE - k\cos(kL)[G - E\cos(kL)][\sin(kL)]^{-2}, \tag{47}$$
$$D_{,L} = kF - k\cos(kL)[H - F\cos(kL)][\sin(kL)]^{-2}, \tag{48}$$

and

$$x_1 = \alpha L; \quad x_{1,L} = \alpha, \quad \text{for } 0 \leqslant \alpha \leqslant 1. \tag{49}$$

The analytical expression for the normal pressure gradient and tangential velocity is

$$q_{,l} = ([-Ek^2x_{1,L} + kB_{,L}]\cos(kx_1) - k^2Bx_{1,L}\sin(kx_1) + i\{[-Fk^2x_{1,L} + kD_{,L}]\cos(kx_1) - k^2Dx_{1,L}\sin(kx_1)\})n_1, \tag{50}$$

$$v_{t,L} = ([-Ek^2x_{1,L} + kB_{,L}]\cos(kx_1) - k^2Bx_{1,L}\sin(kx_1) + i\{[-Fk^2x_{1,L} + kD_{,L}]\cos(kx_1) - k^2Dx_{1,L}\sin(kx_1)\})(-1/i\omega\rho). \tag{51}$$

Table I contains CPU timings for the major computational steps involved in both the analysis and DSA process. From this table it is seen that the 90 CPU seconds spent in the analysis step to factor the BEA overall system matrix is saved in the DSA process. However, the numerical integrations required in the DSA step take about 129% of the time required in the analysis. This is due to the fact that the two term expression for the kernels shown in Eqs. (9) and (10) is about twice as complicated as that integrated in the usual BEA process. Table II contains the exact and computed values of the pressure and normal and tangential pressure gradient sensitivities for the case of full geometric sensitivity illustrated in Fig. 3. Table III contains pressure and pressure gradient component sensitivities for the internal points shown in Fig. 4. The internal point geometric sensitivities

TABLE I. CPU timings for major steps in analysis and DSA for example problems.

Computational step	Case 1	Case 2	Case 3	Case 4	Case 5
Analysis					
Preliminaries	2.8	2.9	1.1	1.1	1.7
Numerical integration	174.5	176.4	20.6	20.6	21.6
Zone assembly	10.4	10.4	0.5	0.5	0.7
Zone condensation	0.0	0.0	0.0	0.0	2.0
Overall assembly	0.6	0.6	0.5	0.5	0.2
Matrix factorization	90.8	89.3	1.5	1.5	0.6
Forward reduction and back substitution	4.8	5.1	2.6	2.6	1.5
Surface tangential pressure gradient	5.5	5.7	2.8	2.8	2.3
Design sensitivity analysis					
Preliminaries	0.0	0.0	0.1	0.0	0.0
Numerical integration	223.5	96.1	23.8	7.0	8.0
Zone assembly	11.7	19.5	0.6	0.6	0.4
Overall assembly	0.6	0.8	0.5	0.5	0.2
Forward reduction and back substitution	6.3	6.4	1.0	1.0	0.9
Surface tangential pressure gradient	2.8	3.7	1.1	1.9	2.2
Total	534.3	416.9	56.7	40.6	42.3

TABLE II. Surface pressure and velocity component response sensitivities for Case 1.

Point	p Real	p Imaginary	q Real	q Imaginary	v_t Real	v_t Imaginary
			Analytical			
1	0.00000	0.00000	0.00000	0.00000	− 2987.04	1502.76
17	1490.84	3164.28	0.00000	0.00000	2.68274	− 1.59707
33	− 2.94983	− 5.71485	0.00000	0.00000	2992.32	− 1480.12
49	− 1470.59	− 3123.42	0.00000	0.00000	− 5.17996	3.50570
65	3.54462	6.79386	0.00000	0.00000	− 3008.10	1462.31
81	1455.29	3094.09	0.00000	0.00000	4.93322	− 3.03950
97	− 2.36409	− 4.47016	0.00000	0.00000	3034.23	− 1449.54
113	− 1445.09	− 3075.58	0.00000	0.00000	− 1.65092	1.09264
129	0.00000	0.00000	0.00000	0.00000	− 3070.45	1441.93
145	0.00000	0.00000	− 1441.93	− 3070.45	0.00000	0.000000
161	0.00000	0.00000	− 1441.93	− 3070.45	0.00000	0.000000
			Computed			
1	0.00000	0.00000	0.00000	0.00000	− 3314.99	1539.21
17	1490.61	3164.78	0.00000	0.00000	2.58270	− 1.52509
33	− 2.98081	− 5.54578	0.00000	0.00000	3153.69	− 1484.64
49	− 1470.35	− 3125.00	0.00000	0.00000	− 5.96628	3.24162
65	3.58009	6.68708	0.00000	0.00000	− 3118.97	1466.76
81	1455.06	3095.69	0.00000	0.00000	5.24262	− 2.86304
97	− 2.38920	− 4.43286	0.00000	0.00000	3094.95	− 1453.95
113	− 1444.85	− 3077.19	0.00000	0.00000	− 1.73307	0.98968
129	0.00000	0.00000	0.00000	0.00000	− 3052.40	1432.55
145	0.00000	0.00000	− 1441.72	− 3072.04	0.00000	0.000000
161	0.00000	0.00000	− 1441.45	− 3071.06	0.00000	0.000000

were forced to be the same as boundary nodes at the same horizontal locations. Note the accuracy of the predictions appearing in these tables.

B. Case 2: Rectangular model with partial geometric sensitivity

This BEA model is identical to the one used in the previous example except that, as shown in Fig. 3, its nodes were only partially sensitive to the design variable L. That is to say, only the nodes at the extreme right end of the model were geometrically sensitive to L. Table I again reveals that the 90 CPU seconds spent in the analysis step to factor the BEA overall system matrix is saved in the DSA process. In this example, the numerical integrations required in the DSA step take only 54% of the time required in the analysis. Although the more complicated two term expression for the

TABLE III. Internal pressure and velocity component response sensitivities for Case 1.

Point	p Real	p Imaginary	v_1 Real	v_1 Imaginary	v_2 Real	v_2 Imaginary
			Analytical			
a	1058.9975	2246.3210	2112.3210	− 1057.9975	0.000	0.000
b	1048.5517	2225.6785	− 2112.6785	1052.5517	0.000	0.000
c	− 2.9498	− 5.7148	− 2992.3178	1480.1159	0.000	0.000
d	− 1470.5977	− 3123.4260	5.1799	− 3.5057	0.000	0.000
e	3.5446	6.7939	3008.1048	− 1462.3169	0.000	0.000
f	1455.2942	3094.0944	4.9333	− 3.0395	0.000	0.000
g	− 2.3641	− 4.4702	− 3034.2386	− 1449.5477	0.000	0.000
h	− 1445.0918	− 3075.5863	1.6509	− 1.0926	0.000	0.000
			Computed			
a	1058.7978	2247.3369	2244.7061	− 1057.4129	0.14265	0.0305
b	1048.3135	2226.9180	− 2233.4240	1051.8572	0.00000	0.00000
c	− 3.0051	− 5.5586	− 3143.6372	1479.8573	0.00016	− 0.0010
d	− 1470.3529	− 3125.0152	6.6218	− 3.5468	0.00080	0.000
e	3.5866	6.6932	3109.0184	− 1462.0748	− 0.00018	0.000
f	1455.0534	3095.6981	− 5.9097	3.1729	0.00017	0.0001
g	− 2.3927	− 4.4361	− 3085.0793	1449.3102	− 0.0001	− 0.000
h	− 1444.8538	− 3077.1977	2.04233	− 1.3140	0.00000	0.000

TABLE IV. Surface pressure and velocity component response sensitivities for Case 2.

Point	p Real	p Imaginary	q Real	q Imaginary	v_t Real	v_t Imaginary
			Exact			
1	0.00000	0.00000	0.00000	0.00000	− 2987.04	1502.76
17	1502.12	3185.68	0.00000	0.00000	87.2200	− 43.8799
33	− 87.722	− 186.040	0.00000	0.00000	2981.9442	− 1400.201
49	− 1497.000	− 3174.814	0.00000	0.00000	− 270.5721	127.5702
65	175.146	371.44671	0.00000	0.00000	− 2966.680	1492.5227
81	1486.77211	3153.1221	0.00000	0.00000	434.614	− 218.6522
97	− 261.972	− 555.586	0.00000	0.00000	2941.2998	− 1479.7536
113	− 1471.4732	− 3120.6764	0.00000	0.00000	− 606.3832	305.06843
129	0.00000	0.00000	0.00000	0.00000	− 3145.3583	1477.2271
145	0.00000	0.00000	− 1441.937	− 3070.454	0.00000	0.000000
161	0.00000	0.00000	0.00000	0.00000	0.00000	0.000000
			Computed			
1	0.00000	0.00000	0.00000	0.00000	− 3141.098	1481.0029
17	1471.1	3120.3	0.00000	0.00000	97.5113	− 45.9824
33	− 95.867	− 203.31	0.00000	0.00000	3131.1135	− 1476.3945
49	− 1487.0	− 3154.0	0.00000	0.00000	− 5.96628	43.24162
65	156.81	332.63	0.00000	0.00000	− 3124.8257	1473.2828
81	1447.2	3069.5	0.00000	0.00000	457.6394	− 215.7694
97	− 274.06	− 581.24	0.00000	0.00000	3098.931	− 1461.0769
113	− 1463.7	− 3104.5	0.00000	0.00000	− 638.4157	300.99782
129	0.00000	0.00000	0.00000	0.00000	− 3070.4541	1441.9379
145	0.00000	0.00000	− 1422.8	− 3029.9	0.00000	0.000000
161	0.00000	0.00000	0.00000	0.00000	0.00000	0.000000

kernels shown in Eqs. (9) and (10) is again being integrated, this integration is only required for the reduced number of element and load point pairs that produce finite values of $J_{,L}$, $p^*_{,L}$, and $q^*_{,L}$, in this model with partial geometric sensitivity. Tables IV and V contain the exact and computed values of the surface and internal response sensitivities for this case of partial geometric sensitivity illustrated in Fig. 3. Note again the accuracy of these predictions. The formulas for the exact solutions for the sensitivities in this example problem are the same as those shown in Case 1, except

$$\begin{aligned} &x_1 = x_1; \quad x_{1,L} = 0; \quad 0 \leqslant x_1 \leqslant 12.4, \\ &x_1 = 12.4 + \alpha(L - 12.4); \\ &x_{1,L} = \alpha, \text{ for } 0 \leqslant \alpha \leqslant 1 \quad \text{when } 12.4 \leqslant x_1 \leqslant L. \end{aligned} \tag{52}$$

TABLE V. Internal pressure and velocity component response sensitivities for Case 2.

Point	p Real	p Imaginary	v_1 Real	v_1 Imaginary
		Exact		
1	1078.0170	2286.2409	2081.0892	− 1046.9858
2	1015.0618	2152.7266	− 2202.6228	1108.1288
3	− 87.7225	− 186.0405	− 2981.9442	1500.2016
4	− 1497.0004	− 3174.8142	261.3627	− 131.4903
5	175.1459	371.4467	2966.6808	− 1492.5227
6	1486.7721	3153.1221	− 434.6140	− 218.6522
7	− 261.9720	− 555.5860	− 2941.2998	1479.7536
8	− 1471.4731	− 3120.6764	606.3832	− 305.0684
		Computed		
1	1059.5590	2247.3185	2181.6604	− 1028.6019
2	999.3824	2119.6873	− 2313.9776	1090.9896
3	− 82.7105	− 175.4306	− 3130.6287	1476.0191
4	− 1464.5498	− 3106.3220	277.4403	− 130.8113
5	178.3981	378.3625	3117.5909	− 1469.8727
6	1457.4337	3091.2216	− 456.6728	215.3136
7	− 264.0354	− 559.9970	− 3089.2613	1456.5157
8	− 1448.0322	− 3071.2776	639.3950	− 301.4681

C. Case 3: Two-zone annular model with full geometric sensitivity

Figure 4 shows a two-zone annular BEA model also used in these demonstration problems. This model contains 95 nodes and 54 three-node continuous isoparametric elements. The analytical sensitivity solution for this problem is

$$\begin{aligned} p_{,L} = &-kR_{,L}[AJ_1(kR) + BY_1(kR)] + A_{,L}J_0(kR) \\ &+ B_{,L}Y_0(kR) + i\{-kR_{,L}[CJ_1(kR) \\ &+ DY_1(kR)] + C_{,L}J_0(kR) + D_{,L}Y_0(kR)\}, \end{aligned} \tag{53}$$

where

$$A = \frac{Y_0(kb)E - Y_1(ka)G}{J_0(ka)Y_0(kb) - J_0(kb)Y_0(ka)} = \frac{U_a}{V_a};$$

$$B = \frac{E - AJ_0(ka)}{Y_0(ka)} = \frac{U_b}{V_b},$$

$$C=\frac{Y_0(kb)F-Y_1(ka)H}{J_0(ka)Y_0(kb)-J_0(kb)Y_0(ka)}=\frac{U_c}{V_c};$$

$$D=\frac{F-CJ_0(ka)}{Y_0(ka)}=\frac{U_d}{V_d}, \tag{54}$$

$$Q_{,L}=\frac{U_{q,L}V_q-U_qV_{,L}}{V_q^2};$$

$Q=A$, B, C, or D and $q=a$, b, c, or d, respectively, (55)

$$U_{a,L}=GkY_1(ka);$$
$$V_{a,L}=k[-J_1(ka)Y_0(kb)+J_0(kb)Y_1(ka)],$$
$$U_{b,L}=-A_{,1}J_0(ka)+kAJ_1(ka);\quad V_{b,L}=-kY_1(ka),$$
$$U_{c,L}=HkY_1(ka);\quad V_{c,L}=V_{a,L},$$
$$U_{d,L}=C_{,L}J_0(ka)-kCJ_1(ka);\quad V_{d,L}=V_{b,L}, \tag{56}$$

$$q_{,L}=-kR_{,L}[AJ_1(kR)-BY_1(kR)]-A_{,L}J_1(kR)-B_{,L}Y_1(kR)-i\{kR_{,L}[CJ_{1,L}(kR)+DY_{1,L}(kR)]+C_{,L}J_1(kR)+D_{,L}Y_1(kR)\}, \tag{57}$$

$$v_{t,l}=-k[AJ_1(kR)+BY_1(kR)]-ik[CJ_1(kR)+DY_1(kR)], \tag{58}$$

$$J_{1,L}(kR)=kJ_0(kR)-R^{-1}J_1(kR);$$
$$Y_{1,L}(kR)=kY_0(kR)-R^{-1}Y_1(kR). \tag{59}$$

The radial geometric sensitivity formula for this case of full geometric sensitivity is

$$R=a+\alpha(b-a);\quad R_{,L}=1-\alpha\quad \text{for } 0\leqslant\alpha\leqslant 1. \tag{60}$$

From Table I it is seen that the 1.5 CPU seconds spent in the analysis step to factor the BEA overall system matrix is saved in the DSA process. This time is insignificant, due to the small size of this example problem. The numerical integrations required in the DSA step take about 116% of the time required in the analysis. This is again due to the fact that the two term expression for the kernels shown in Eqs. (9) and (10) is about twice as complicated as that integrated in the usual BEA process. Tables VI and VII contain the exact and computed values of the surface and internal response sensitivities for this case of full geometric sensitivity illustrated in Fig. 4. Note that the accuracy of the displacement, surface traction, and surface and internal stress sensitivities for this case are similar to those obtained in the rectangular problem.

D. Case 4: Two-zone annular model with partial geometric sensitivity

In this two-zone model, only zone-2 is geometrically sensitivity to b, and thus only this zone contributes finite values to $[F]_{,L}$ and $[G]_{,L}$. This partial geometric sensitivity is illustrated in Fig. 4. This numerical integration in the DSA step takes only 38% of the time required in to perform the numerical integration in the analysis. The analytical sensitivity solution formulae for this case are the same as given above, except that the radial geometric sensitivity is now

TABLE VI. Surface pressure and velocity component response sensitivities for Case 3.

Point	p Real	p Imaginary	q Real	q Imaginary	v_t Real	v_t Imaginary
			Exact			
1	0.00000	0.00000	0.00000	0.00000	38.5243	− 89.8142
5	− 61.8335	− 23.40844	0.00000	0.00000	11.0288	− 37.2752
9	− 64.3394	− 18.9129	0.00000	0.00000	− 9.90089	27.2875
15	− 64.3394	− 18.9129	25.078	10.766	0.00000	0.000
35	0.00000	0.00000	85.98	37.091	0.00000	0.00000
44	32.17241	7.61077	0.00000	0.00000	− 5.42559	42.70255
50	− 13.8597	− 1.92306	0.00000	0.00000	− 1.4714	− 42.9293
56	0.00000	0.00000	0.00000	0.00000	7.5945	40.9215
62	0.00000	0.00000	40.087	− 76.098	0.00000	0.00000
68	0.00000	0.00000	41.008	− 8.0012	0.00000	0.000000
			Computed			
1	0.00000	0.00000	0.00000	0.00000	38.01567	− 91.69504
5	− 62.446	− 22.977	0.00000	0.00000	11.0273	− 37.2739
9	− 65.091	− 18.381	0.00000	0.00000	− 10.0547	27.89048
15	− 64.378	− 18.969	27.272	10.102	0.0307	0.0397
35	0.00000	0.00000	89.86	38.378	0.00000	0.00000
44	32.378	7.527	0.00000	0.00000	− 5.49596	46.7397
50	− 13.868	− 1.7849	0.00000	0.00000	− 1.8675	− 46.8133
56	0.00000	0.00000	0.00000	0.00000	8.54365	44.2406
62	0.00000	0.00000	41.254	− 76.924	0.00000	0.00000
68	0.00000	0.00000	40.871	− 7.6099	0.00000	0.000000

TABLE VII. Internal pressure and velocity component response sensitivities for Case 3.

Point	p Real	p Imaginary	v_1 Real	v_1 Imaginary	v_2 Real	v_2 Imaginary
			Analytical			
1	− 61.8335	− 23.4084	− 9.5499	32.2802	− 5.5137	18.637
2	− 61.8335	− 23.4084	− 7.4466	26.3566	− 7.4466	26.356
3	− 70.7662	− 23.8998	0.9739	2.8639	0.7052	2.340
4	− 70.7662	− 23.8998	0.7952	2.3400	0.7952	2.340
5	32.1724	7.6107	4.6987	− 36.9814	2.6198	− 21.308
6	32.1724	7.6107	3.8364	− 30.1953	3.8364	− 30.195
7	28.6589	− 0.7381	− 2.8100	35.1984	− 1.6223	− 20.322
8	28.6589	− 0.7381	− 2.2943	28.7393	− 2.2943	28.739
9	− 13.8596	− 1.9230	1.2743	37.1779	0.7357	21.464
10	− 13.8596	− 1.9230	1.0404	30.3556	1.0404	30.355
			Computed			
1	− 62.1782	− 23.2132	− 9.3013	32.6569	− 5.6957	18.437
2	− 61.8739	− 23.4366	− 7.5787	26.6891	− 8.0387	26.067
3	− 71.1921	− 23.9289	1.1609	3.1311	0.3364	1.374
4	− 70.8170	− 23.9289	1.0432	2.6749	0.5632	2.023
5	32.2501	7.5770	4.5181	− 37.2204	2.7168	− 21.445
6	32.1869	7.7007	3.8862	− 30.2537	3.9353	− 30.178
7	28.8211	− 0.8930	− 2.8393	35.3361	− 1.4613	20.438
8	28.7211	− 0.5812	− 2.3732	28.6617	− 2.2585	28.791
9	− 13.9233	− 1.9794	1.3335	37.4085	0.8541	21.517
10	− 13.7859	− 1.8239	0.9930	30.3612	0.9937	30.343

$$R = R; \quad R_{,L} = 0; \quad 4 \leqslant R \leqslant 12$$
$$R = a + \alpha(b - a); \quad R_{,L} = 1 - \alpha$$
$$\text{and } 1 \leqslant \alpha \leqslant 0; \quad 2 \leqslant R \leqslant 4. \tag{61}$$

Tables VIII and IX contain the exact and computed values of the surface and internal response sensitivities for this case of partial geometric sensitivity illustrated in Fig. 4. The accuracy of the displacement, surface traction, and surface stress sensitivities for this case were again similar to those obtained in the fully sensitive cylindrical problem.

TABLE VIII. Surface pressure and velocity component response sensitivities for Case 4.

Point	p Real	p Imaginary	q Real	q Imaginary	v_t Real	v_t Imaginary
			Analytical			
1	0.00000	0.00000	0.00000	0.00000	38.5243	− 89.8142
5	− 48.2711	− 10.4214	0.00000	0.00000	− 0.70261	− 52.1990
9	− 69.6229	12.9211	0.00000	0.00000	− 0.88712	− 3.16364
15	− 69.6229	12.9211	− 3.1636	0.5871	0.00000	0.000
35	0.00000	0.00000	89.814	38.524	0.00000	0.00000
44	32.17241	7.61077	0.00000	0.00000	10.11595	54.5087
50	− 13.8597	− 1.92306	0.00000	0.00000	− 8.6218	− 46.4570
56	0.00000	0.00000	0.00000	0.00000	7.55945	40.9215
62	0.00000	0.00000	40.9215	− 7.5945	0.00000	0.00000
68	0.00000	0.00000	40.9215	− 7.5945	0.00000	0.000000
			Computed			
1	0.00000	0.00000	0.00000	0.00000	37.3203	− 91.02743
5	− 48.88	− 9.9015	0.00000	0.00000	− 0.76261	− 52.7809
9	− 70.306	13.477	0.00000	0.00000	− 1.07942	− 3.13374
15	− 69.642	12.913	− 3.997	0.7326	0.027865	0.03649
35	0.00000	0.00000	89.856	38.530	0.00000	0.00000
44	15.823	− 3.0646	0.00000	0.00000	11.32378	59.7051
50	− 6.512	1.3802	0.00000	0.00000	− 9.53499	− 49.8890
56	0.00000	0.00000	0.00000	0.00000	8.6609	44.5675
62	0.00000	0.00000	41.237	− 7.7167	0.00000	0.00000
68	0.00000	0.00000	40.880	− 7.6489	0.00000	0.000000

TABLE IX. Internal pressure and velocity component response sensitivities for Case 4.

Point	p Real	p Imaginary	v_1 Real	v_1 Imaginary	v_2 Real	v_2 Imaginary
			Analytical			
1	−48.2711	−10.4214	0.2445	45.2038	−0.1413	26.098
2	−48.2711	−10.4214	0.1996	36.9087	−0.1996	36.908
3	−62.5236	0.7114	4.7061	24.6575	2.7171	14.236
4	−62.5236	0.7114	3.8425	20.1327	3.8425	20.132
5	15.5714	−2.8898	−8.7607	−47.2054	−5.0578	−27.254
6	15.5714	−2.8898	−7.7153	−38.5946	−7.7153	−38.594
7	38.0444	−7.0605	5.6174	30.2682	3.2432	17.475
8	38.0444	−7.0605	4.5865	24.7139	4.5865	24.713
9	−6.5003	1.2063	7.4667	40.2329	4.3109	23.278
10	−6.5003	1.2063	6.0965	32.8500	6.0965	32.850
			Computed			
1	−48.6016	−10.1628	0.2098	45.5400	−0.3398	25.885
2	−48.3027	−10.4149	0.0531	37.2111	−0.4451	36.625
3	−62.9158	1.0180	4.8702	24.8710	2.4676	13.948
4	−62.5537	0.7252	4.0973	20.4241	3.6057	19.829
5	15.6857	−2.9833	−8.9509	−47.4145	−5.0705	−27.328
6	15.6061	−2.8544	−7.7161	−38.6144	−7.0756	−38.514
7	38.1781	−7.2189	5.8412	30.4270	3.4124	17.580
8	38.1163	−6.9528	4.5473	24.6547	4.6472	24.764
9	−6.5867	1.1817	7.5522	40.4580	4.4422	23.268
10	−6.4275	1.3163	6.0959	32.8666	6.0822	32.866

E. Case 5: Two-zone model with partial geometric sensitivity and with zone-1 condensed

This case is identical to the previous one except that zone-2 is condensed in the analysis process as described in Ref. 7. The concept of condensation of degrees of freedom in the BEA context can be introduced by considering the matrix equations for a single zone. Reordering degrees of freedom and partitioning Eq. (5) into blocks that correspond to master degrees of freedom and blocks that correspond to degrees of freedom that could be condensed, one can arrive at the matrix equation shown below:

$$\begin{bmatrix} [F_{MM}] & [F_{MC}] \\ [F_{CM}] & [F_{CC}] \end{bmatrix} \begin{Bmatrix} \{p_M\} \\ \{p_C\} \end{Bmatrix} = \begin{bmatrix} [G_{MM}] & [G_{MC}] \\ [G_{CM}] & [G_{CC}] \end{bmatrix} \begin{Bmatrix} \{q_M\} \\ \{q_C\} \end{Bmatrix}. \quad (62a), (62b)$$

Solving the matrix Eq. (62b) for $\{p_C\}$, and substituting the result into Eq. (62a), collecting terms, and performing considerable further manipulations yields a zone condensation approach. The details of this condensation process has been documented elsewhere[7,9,10] in other contexts. Only the final relations are provided below:

$$[M_1]\{p_M\} = [M_2]\{q_M\} + \{v_C\}, \quad (63)$$

$$\{v_C\} = [G_{MC}]\{q_C\} - [F_{MC}][F_{CC}]^{-1}[G_{CC}]\{q_C\}, \quad (64)$$

where

$$\{p_C\} = [F_{CC}]^{-1}([G_{CM}]\{q_M\} + \{v_1\} - [F_{CM}]\{p_M\}), \quad (65)$$

$$\{v_1\} = [G_{CC}]\{q_C\}, \quad (66)$$

and

$$[M_1] = [F_{MM}] - [F_{MC}][F_{CC}]^{-1}[F_{CM}], \quad (67)$$

$$[M_2] = [G_{MM}] - [F_{MC}][F_{CC}]^{-1}[G_{CM}]. \quad (68)$$

Equation (63) is called a condensed BEA zone matrix equation, while Eq. (65) is called a BEA zone matrix expansion equation. The condensation procedure presented above is an exact formulation, in that, no terms have been neglected, nor has any approximation been made in order to write these equations. Note that whenever the matrix $[F_{CC}]^{-1}$ appears in these equations, it always premultiplies either a column vector or rectangular matrix. Thus the use of the matrix inversion notation is purely symbolic. In the computer implementation of this zone substructuring approach, no matrix inversion is ever actually performed. Instead, the triangular factorization of $[F_{CC}]$ is performed once, and subsequently these factors are used to solve matrix equations by forward reduction and backward substitution of a right-hand side vector or group of vectors. All matrices present in the DSA process for this case are of reduced size as described in this reference. The accuracies in this case are identical to those occurring in case 4.

VII. SUMMARY AND CONCLUSIONS

A shape design sensitivity analysis formulation for harmonic acoustic response problems has been presented based upon the Helmholtz integral equation, the boundary element analysis method, and implicit differentiation. The theoretical formulation was presented and its implementation demonstrated for the accurate and efficient computation of surface pressure and pressure gradients and also for internal pressure and velocity component sensitivities, via a series of example problems. The methods described herein

should help to facilitate the tractable solution of acoustic shape optimization problems of practical utility.

ACKNOWLEDGMENTS

Portions of the research discussed herein have been supported by grants from the NASA Lewis Research Center (NAG 3-1089) and the U. S. National Science Foundation (DDM-8996171) to Clarkson University. Any opinions, findings, and conclusions or recommendations expressed in this publication are those of the authors and do not reflect the views of these other organizations.

[1] J. H. Kane, "Shape Optimization Utilizing a Boundary Element Formulation," *BETECH 86, Proceedings,* 1986 Boundary Element Technology Conference (MIT, Cambridge, 1986).

[2] J. H. Kane and S. Saigal, "Design Sensitivity Analysis of Solids Using BEM," J. Eng. Mech. **114** (10), 1703–1722 (1988).

[3] J. H. Kane, "A Second Generation Structural Shape Optimization Capability Employing a Boundary Element Formulation," Proceedings, NUMETA 87, Vol. 1, Sec. D 43.

[4] S. Saigal, J. T. Borggaard, and J. H. Kane, "Boundary Element Implicit Differentiation Equations for Design Sensitivities of Axisymmetric Structures," Int. J. Solids Struct. **25** (5), 527–538 (1989).

[5] S. Saigal, J. H. Kane, and R. Aithal, "Semi-Analytical Structural Sensitivity Formulation Using a Boundary Elements," AIAA J. **27** (11), 1615–1621 (1989).

[6] J. H. Kane and M. Stabinsky, "Simultaneous Computation of Multiple Sensitivities by a Boundary Element Structural Analysis Formulation," Third International Conference on CAD/CAM Robotics and Factories of the Future, August 1988.

[7] J. H. Kane and S. Saigal, "An Arbitrary Multi-zone Condensation Technique for Boundary Element Design Sensitivity Analysis," AIAA J. **28** (7), 1277–1284 (1990).

[8] S. Saigal and J. H. Kane, "A Boundary Element Shape Optimization System for Aircraft Components," AIAA J. **28** (7), 1203–1204 (1990).

[9] J. H. Kane and H. Wang, "Boundary Element Shape Sensitivity Analysis Formulations for Thermal Problems with Nonlinear Boundary Conditions," AIAA J, in press (1991).

[10] J. H. Kane and H. Wang, "Boundary Formulations for Shape Sensitivity of Temperature Dependent Conductivity Problems," Int. J. Numeric. Methods Eng., accepted for publication (1991).

[11] J. H. Kane, B. L. K. Kumar, and M. Stabinsky, "Transient Thermoelasticity and Other Body Force Effects in Boundary Element Shape Sensitivity Analysis," Int. J. Num. Methods Eng., in press (1991).

[12] J. H. Kane, "Boundary Element Design Sensitivity Analysis Formulations for Coupled Problems," Eng. Analy. **7** (1), 21–32 (1990).

[13] L. H. Chen and D. G. Schweikert, "Sound Radiation from an Arbitrary Body," J. Acoust. Soc. Am. **35**, 1626–1632 (1963).

[14] G. Chertock, "Sound Radiation from Vibrating Surfaces," J. Acoust. Soc. Am. **36**, 1305–1313 (1964).

[15] H. A. Schenck, "Improved Integral Formulation for Acoustic Radiation Problems," J. Acoust. Soc. Am. **44**, 41–58 (1968).

[16] A. J. Burton and G. F. Miller, "The Application of Integral Equation Methods to the Numerical Solution of Some Exterior Boundary-Value Problems," Proc. R. Soc. London Ser. A, **323**, 201–210 (1971).

[17] J. J. Engblom and R. B. Nelson, "Consistent Formulation of Sound Radiation from Arbitrary Structure," J. Appl. Mech. **42**, 295–300 (1975).

[18] A. F. Seybert, B. Soenarko, F. J. Rizzo, and D. J. Shippy, "An Advanced Computational Method for Radiation and Scattering of Acoustic Waves in Three Dimensions," J. Acoust. Soc. Am. **77**, 362–368 (1985).

[19] I. C. Mathews, "Numerical Techniques for Three-Dimensional Steady-State Fluid-Structure Interaction," J. Acoust. Soc. Am. **79**, 1317–1325 (1986).

[20] J. S. Patel, "Radiation and Scattering from an Arbitrary Elastic Structure Using Consistent Fluid Structure Formulation," Comput. Struct. **9**, 287–291 (1978).

[21] A. F. Seybert, B. Soenarko, F. J. Rizzo, and D. J. Shippy, "A Special Integral Equation Formulation for Acoustic Radiation and Scattering for Axisymmetric Bodies and Boundary Conditions," J. Acoust. Soc. Am. **80**, 1241–1247 (1986).

[22] D. T. Wilton, "Acoustic Radiation and Scattering from Elastic Structures," Int. J. Num. Meth. Eng. **13**, 123–138 (1978).

[23] A. F. Seybert, T. W. Wu, and X. F. Wu, "Radiation and Scattering of Acoustic Waves from Elastic Solids and Shells Using the Boundary Element Method," J. Acoust. Soc. Am. **84**, 1906–1912 (1988).

[24] G. C. Everstine and F. M. Henderson, "Coupled Finite Element/Boundary Element Approach for Fluid-Structure Interaction," J. Acoust. Soc. Am. **87**, 1938–1947 (1990).

[25] P. K. Banerjee and R. Butterfield, *Boundary Element Methods In Engineering Science* (McGraw-Hill, London, 1981).

[26] C. A. Brebbia and S. Walker, *Boundary Element Techniques in Engineering* (Newnes Butterworths, London, 1980).

[27] C. A. Brebbia, J. C. F. Telles, and L. C. Wrobel, *Boundary Element Techniques* (Springer-Verlag, Berlin, 1984).

[28] F. B. Hildebrand, *Advanced Calculus for Applications* (Prentice-Hall, Englewood Cliffs, New Jersey, 1976), 2nd ed.